J|A|C|S ARTICLES

Published on Web 10/01/2009

Phase Selection and Energetics in Chiral Alkaline Earth Tartrates and Their Racemic and *Meso* Analogues: Synthetic, Structural, Computational, and Calorimetric Studies

Leah N. Appelhans,[†] Monica Kosa,[‡] A. V. Radha,[§] Petra Simoncic,[§] Alexandra Navrotsky,*[,§] Michele Parrinello,*[,‡] and Anthony K. Cheetham*[,||]

Solid State Lighting and Energy Center, University of California, Santa Barbara, California 93106, Computational Science, Department of Chemistry, and Applied Biosciences, ETH Zurich, c/o USI Campus, Via Giuseppe Buffi 13, CH-6900 Lugano, Switzerland, Peter A. Rock Thermochemistry Laboratory and NEAT-ORU, University of California, One Shield Avenue, Davis, California 95616, and Department of Materials Science and Metallurgy, University of Cambridge, Pembroke Street, Cambridge CB2 3QZ, U.K.

Received July 15, 2009; E-mail: anavrotsky@ucdavis.edu; parrinello@phys.chem.ethz.ch; akc30@cam.ac.uk

Abstract: The hydrothermal reactions of calcium, strontium, and barium with L-, *meso*-, and D,L-tartaric acid were examined from room temperature to 220 °C. We report the synthesis of 13 new phases and crystal structures of 11 alkaline earth tartrates, including an unusual I^3O^0 framework, [Ba(D,L-Tar)] (Tar = $C_4H_4O_6^{2-}$), with 3-D inorganic connectivity. Each alkaline earth exhibits different phase behavior in the reactions with the three forms of tartaric acid. Calcium forms unique L-, *meso*-, and D,L-tartrate phases which persist to 220 °C. Strontium forms three unique phases at lower temperatures, but above 180 °C reactions with L- and D,L-tartaric acid yield the *meso* phase. Likewise, Ba forms three unique low-temperature phases, but above 200 °C reactions with L- and *meso*-tartaric acid yield the D,L phase. Computational and calorimetric studies of the anhydrous calcium phases, [Ca(L-Tar)] and [Ca(*meso*-Tar)], strontium phases, [Sr(L-Tar)] and [Sr(*meso*-Tar)], and barium phases, [Ba(L-Tar)] and [Ba(D,L-Tar)], were performed to determine relative phase stabilities and elucidate the role of thermodynamic and kinetic factors in controlling phase behavior. The computational and calorimetric results were in excellent agreement. The [Ca(*meso*-Tar)] phase was found to be 9.1 kJ/mol more stable than the [Ca(L-Tar)] phase by computation (total electronic energies) and 2.9 ± 1.6 kJ/mol more stable by calorimetry (enthalpies of solution). The [Sr(*meso*-Tar)] phase was found to be 13.4 and 8.1 ± 1.4 kJ/mol more stable than [Sr(L-Tar)] by computation and calorimetry, respectively. Finally, the [Ba(L-Tar)] phase was found to be 6.4 and 7.0 ± 1.0 kJ/mol more stable than the [Ba(D,L-Tar)] phase. Our results suggest that the calcium and strontium *meso* phases are the most thermodynamically stable phases in their systems over the temperature range studied. The phase transitions are controlled by relative thermodynamic stabilities but also by a kinetic factor, likely the barrier to isomerization/racemization of the tartaric acid, which is hypothesized to preclude phase transformations at lower temperatures. In the barium system we find the [Ba(L-Tar)] phase to be the most thermodynamically stable phase at low temperatures, while the [Ba(D,L-Tar)] phase becomes the thermodynamic product at high temperatures, due to a larger entropic contribution.

Introduction

Interest in the synthesis of chiral metal−organic frameworks[1−3] has led to the increasing use of naturally derived chiral building blocks, particularly carboxylic acids, for chiral framework synthesis. The use of a chiral, enantiopure ligand is the most fail-safe method for synthesizing chiral extended solids since, unless the ligand racemizes, the resulting metal−organic framework must also be chiral. While any chiral ligand that is stable to the reaction conditions can be used,[4,5] amino acids and other naturally derived carboxylic acids have the distinct advantage of being available as the pure enantiomers, relatively cheap, and easy to obtain. A number of recent studies have used these types of ligands to reliably synthesize chiral frameworks.[6−12] Although obtaining a chiral framework from chiral building

[†] University of California, Santa Barbara.
[‡] ETH Zurich.
[§] University of California, Davis.
[||] University of Cambridge.

(1) Bradshaw, D.; Claridge, J. B.; Cuseen, E. J.; Prior, T. J.; Rosseinsky, M. J. *Acc. Chem. Res.* **2005**, *38*, 273.
(2) Lin, W. B. *J. Solid State Chem.* **2005**, *178*, 2486.
(3) Ma, L.; Abney, C.; Lin, W. *Chem. Soc. Rev.* **2009**, *38*, 1248.
(4) Cho, S. H.; Ma, B. Q.; Nguyen, S. T.; Hupp, J. T.; Albrecht-Schmitt, T. E. *Chem. Commun.* **2006**, 2563.
(5) Cui, Y.; Evans, O. R.; Ngo, H. L.; White, P. S.; Lin, W. B. *Angew. Chem., Int. Ed.* **2002**, *41*, 1159.
(6) Anokhina, E. V.; Go, Y. B.; Lee, Y.; Vogt, T.; Jacobson, A. J. *J. Am. Chem. Soc.* **2006**, *128*, 9957.
(7) Barja, B.; Baggio, R.; Calvo, R.; Garland, M. T.; Perec, M.; Rizzi, A. *Inorg. Chim. Acta* **2006**, *359*, 3921.
(8) Thuery, P. *CrystEngComm* **2007**, *9*, 460.
(9) Zhang, J.; Yao, Y. G.; Bu, X. H. *Chem. Mater.* **2007**, *19*, 5083.

blocks is relatively straightforward, understanding and controlling the factors that affect the structures and properties of both chiral and achiral metal−organic frameworks remains a fundamental challenge in the field. Structural control is best exercised in systems that combine a geometrically rigid ligand and a metal with a well-defined coordination geometry. Flexible, polydentate ligands, like many of the natural carboxylic acids, have less predictable structural behavior. Composition and structure, as would be expected, also depend on an array of synthetic variables, and some general trends in hydration and connectivity have been identified.[13] The prediction and control of structure is further complicated because reactions can occur under either thermodynamic or kinetic control.[14,15] In chiral systems, the additional complications of ligand racemization[16] and conglomerate formation are also important. Finally, the existence (or nonexistence) of a predictable structural relationship between chiral and racemic frameworks is also of considerable interest.[9,12,14,17] Series of readily accessible frameworks based on available chiral ligands are ideal systems to advance the understanding of these areas.

Subsequent to our previous work[18] on magnesium tartrates, in which we found that the magnesium tartrate system exhibited unexpected complexity, we became interested in studying the other alkaline earth tartrates in order to better understand the importance of ligand chirality, cation identity, and thermodynamic and kinetic factors in controlling phase diversity and behavior. The study of tartaric acid and its salts has a long history, and as early as 1935 the space group of the enantiopure room-temperature phase, calcium tartrate tetrahydrate, was determined.[19] Complete structures of calcium tartrate tetrahydrate and strontium tartrate trihydrate were subsequently reported in 1968.[20] Despite this early start, the investigation of new alkaline earth tartrates has been limited and continues to focus on room-temperature phases. The room-temperature barium tartrate phase has been synthesized and its structure determined[21] and the structure of the room-temperature phase, strontium tartrate tetrahydrate, solved.[22] However, even with this recent work, only five unique structures of calcium, strontium, and barium tartrates were collected in the CCDC prior to this work. In this work we describe a comprehensive study of the synthesis of a series of calcium, strontium, and barium tartrate frameworks from room temperature to 220 °C. The results reveal a very rich and complex system, generating 13 new phases, with unique phase behavior for each of the metals. By the combination of synthetic, calorimetric, and computational studies, we have been able to identify and begin to distinguish the kinetic and thermodynamic factors controlling phase behavior in this complex system. We focus in particular on the anhydrous phases of Ca, Sr, and Ba, allowing the determination of relative stabilities by computational methods without the complications arising from different levels of hydration.

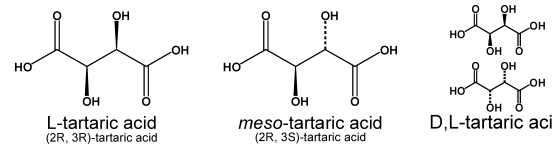

Figure 1. The three forms of tartaric acid.

Results and Discussion

1. Hydrothermal Synthesis of Alkaline Earth Tartrates. The reactions of tartaric acid with calcium, strontium, and barium were studied from room temperature to 220 °C. Tartaric acid exists in three crystalline forms (Figure 1), excluding consideration of polymorphs and hydrates: the chiral D- or L-tartaric acid (*S*,*S*- and *R*,*R*- respectively), the racemic D,L-tartaric acid (racemic mixture of the enantiomers), and the achiral diastereomer, *meso*-tartaric acid (*R*,*S*-tartaric acid). Reactions were carried out with each of the three forms. The reactions yield 18 phases between room temperature and 220 °C, including the five previously known phases. Eleven new crystal structures are reported (Table 1). Structural descriptions of the new anhydrous phases **2**, **7**, **11**, **13**, and **17**, which were used in the computational and calorimetry studies, are included in the text. Complete structural descriptions of all new hydrate phases are included in the Supporting Information.

1.1. Calcium Tartrates. The reactions of calcium acetate with tartaric acid yield seven different phases between room temperature and 220 °C (Table 2). Throughout this paper, connectivity is described using the I^nO^m notation.[13] I^n is the dimensionality of inorganic (metal−oxygen−metal) connectivity. O^m is the dimensionality of organic connectivity, excluding organic connectivity that is redundant with inorganic connectivity. The sum, $n + m$, is the overall connectivity and must be less than or equal to 3. For example, a compound with both 3-D inorganic and 3-D organic connectivity would be described as I^3O^0 because the organic connectivity does not increase the overall connectivity.

Phase Behavior. In the calcium tartrate system, no isomerization of the tartaric acid ligand is observed, even at high temperatures. Calcium forms a unique phase from each of the

(10) Barrio, J. P.; Rebilly, J. N.; Carter, B.; Bradshaw, D.; Bacsa, J.; Ganin, A. Y.; Park, H.; Trewin, A.; Vaidhyanathan, R.; Cooper, A. I.; Warren, J. E.; Rosseinsky, M. J. *Chem.—Eur. J.* **2008**, *14*, 4521.
(11) Zingiryan, A.; Zhang, J.; Bu, X. H. *Inorg. Chem.* **2008**, *47*, 8607.
(12) Anokhina, E. V.; Jacobson, A. J. *J. Am. Chem. Soc.* **2004**, *126*, 3044.
(13) Cheetham, A. K.; Rao, C. N. R.; Feller, R. K. *Chem. Commun.* **2006**, 4780.
(14) Bailey, A. J.; Lee, C.; Feller, R. K.; Orton, J. B.; Mellot-Draznieks, C.; Slater, B.; Harrison, W. T. A.; Simoncic, P.; Navrotsky, A.; Grossel, M. C.; Cheetham, A. K. *Angew. Chem., Int. Ed.* **2008**, *47*, 8634.
(15) Lee, C.; Mellot-Draznieks, C.; Slater, B.; Wu, G.; Harrison, W. T. A.; Rao, C. N. R.; Cheetham, A. K. *Chem. Commun.* **2006**, 2687.
(16) Thushari, S.; Cha, J. A. K.; Sung, H. H. Y.; Chui, S. S. Y.; Leung, A. L. F.; Yen, Y. F.; Williams, I. D. *Chem. Commun.* **2005**, 5515.
(17) Fleck, M.; Tillmanns, E.; Bohaty, L.; Held, P. *Z. Kristallogr.* **2004**, *219*, 101.
(18) Kam, K. C.; Young, K. L. M.; Cheetham, A. K. *Crys. Growth Des.* **2007**, *7*, 1522.
(19) Evans, R. C. *Z. Kristallogr.* **1935**, *92*, 154.
(20) Ambady, G. K. *Acta Crystallogr., Sect. B: Struct. Cryst. Cryst. Chem.* **1968**, *24*, 1548.
(21) Gonzalez-Silgo, C.; Gonzalez-Platas, J.; Ruiz-Perez, C.; Lopez, T.; Torres, M. *Acta Crystallogr, Sect. C: Cryst. Struct. Commun.* **1999**, *55*, 740.
(22) Starynowicz, P.; Meyer, G. *Z. Anorg. Allg. Chem.* **2000**, *626*, 2441.
(23) Sheldrick, G. M. *SHELXTL-97 A Program for Crystal Structure and Refinement*, Ver. 5.1; University of Gottingen: Gottingen, Germany, 1997.
(24) Sheldrick, G. M. *SADABS User Guide*; University of Gottingen: Gottingen, Germany, 1995.
(25) Spek, A. L. *PLATON, A Multipurpose Crystallographic Tool*; University of Utrecht: Utrecht, The Netherlands, 2005.
(26) Flack, H. D. *Acta Crystallogr., Sect. A* **1983**, *39*, 876.
(27) Boese, R.; Heinemann, O. *Z. Kristallogr.* **1993**, *205*, 348.
(28) Hawthorne, F. C.; Borys, I.; Ferguson, R. B. *Acta Crystallogr., Sect. N: Struct. Sci.* **1982**, *38*, 2461.
(29) Devries, A. J.; Kroon, J. *Acta Crystallogr., Sect. C: Cryst. Struct. Commun.* **1984**, *40*, 1542.
(30) Dranka, I.; Lupashku, T.; Shafranskii, V.; Ropot, V.; Kharitonov, Y. Y. *Zh. Neorg. Khim.* **1994**, *39*, 834.
(31) Mastai, Y.; Sedlak, M.; Colfen, H.; Antonietti, M. *Chem.—Eur. J.* **2002**, *8*, 2430.

Table 1. Crystal Data and Structure Refinement[23−26] Parameters for New Alkaline Earth Tartrate Phases

	2	3	7	10	11	12	13	15	16	17	18
identification code	catartm	cadltm	150mcam	srtar60m	ortho2nd	dlsrtpsi	msrtartm	l3188 psi	l3188b	60badl	100mbam2
empirical formula	$C_4H_4CaO_6$	$C_4H_{12}CaO_{10}$	$C_4H_4CaO_6$	$C_4H_6O_7Sr$	$C_4H_4O_6Sr$	$C_4H_{12}O_{10}Sr$	$C_4H_4O_6Sr$	$C_8H_{18}Ba_2O_{17}$	$C_4H_8BaO_8$	$C_4H_4BaO_6$	$C_4H_6BaO_7$
formula wt	188.15	260.22	188.15	253.71	235.69	307.76	235.69	660.9	321.44	285.41	303.43
cryst syst	orthorhombic	triclinic	monoclinic	monoclinic	orthorhombic	triclinic	monoclinic	monoclinic	monoclinic	monoclinic	monoclinic
space group	*C*222(1)	$P\bar{1}$	*C*2/*c*	*P*2(1)	*C*222(1)	$P\bar{1}$	*C*2/*c*	*C*2/*c*	*P*2(1)/*c*	*P*2(1)/*c*	*C*2/*c*
unit cell dimensions											
a (Å)	7.6418(10)	6.2584(15)	17.593(6)	6.6143(5)	7.8865(10)	6.4031(6)	18.306(3)	18.7973(16)	6.4820(7)	8.328(2)	10.8268(7)
b (Å)	9.9656(13)	8.251(2)	7.906(3)	7.1191(5)	10.0448(10)	8.4315(8)	8.0984(13)	5.1127(4)	7.9770(8)	10.116(3)	9.9887(7)
c (Å)	7.2395(9)	10.448(3)	9.462(3)	7.8433(6)	7.5186(8)	10.4933(10)	9.6058(15)	18.5512(16)	16.6234(17)	7.2451(19)	8.5250(6)
α (deg)	90	94.887(6)	90	90	90	95.196(2)	90	90	90	90	90
β (deg)	90	105.914(6)	121.066(5)	98.334(2)	90	106.402(2)	121.334(3)	104.305(2)	95.501(2)	91.338(4)	126.5880(10)
γ (deg)	90	107.662(5)	90	90	90	107.052(2)	90	90	90	90	90
volume (A^3)	551.33(12)	486.0(2)	1127.3(7)	365.42(5)	595.61(12)	510.20(8)	1216.4(3)	1727.6(2)	855.59(15)	610.2(3)	740.27(9)
Z	4	2	8	2	4	2	8	4	4	4	4
d_{calc} (Mg/m^3)	2.267	1.778	2.217	2.306	2.628	2.003	2.574	2.541	2.495	3.107	2.723
reflns collctd	2301	3923	4611	3079	2544	4277	5145	6842	7110	4991	2971
indep reflns	605	1902	1144	1464	637	2003	1306	1822	1813	1281	777
R(int)	0.0661	0.0747	0.0272	0.032	0.0545	0.0375	0.0643	0.0873	0.0248	0.0387	0.0261
absorption correction	SADABS	none	none	SADABS	SADABS	Psi-scan	SADABS	Psi-scan	SADABS	SADABS	SADABS
data/restraints/params	605/2/57	1902/29/172	1144/3/112	1464/5/119	637/1/59	2003/10/172	1306/2/112	1822/12/150	1813/11/142	1281/2/112	777/0/70
GOF	1.063	1.015	1.061	1.069	1.087	1.030	1.045	1.037	1.096	1.074	1.046
final *R* indices [$I > 2\sigma(I)$]											
*R*1	0.0468	0.0517	0.0344	0.0554	0.0265	0.0302	0.0455	0.0375	0.0336	0.0326	0.0214
w*R*2	0.1201	0.1211	0.0822	0.1370	0.0677	0.0680	0.0940	0.0678	0.0850	0.0819	0.0508
R indices (all data)											
*R*1	0.0477	0.0746	0.0410	0.0570	0.0274	0.0384	0.0786	0.0588	0.0419	0.0341	0.0216
w*R*2	0.1213	0.1284	0.0872	0.1392	0.0683	0.0705	0.1081	0.0720	0.0904	0.0831	0.0509
Flack param	0.00(9)			−0.050(18)	−0.036(16)						

Table 2. Reactions between $Ca(OAc)_2$ and Tartaric Acid[a]

temp (°C)	Ca		
	L-Tar (L)	D,L-Tar (DL)	*meso*-Tar (*m*)
rt	$Ca(L)(H_2O)_2 \cdot 2H_2O$ (**1**)[b] I^0O^3 2/2 234.6	$Ca(DL)(H_2O)_4$ (**3**)[c] I^0O^1 4/0 243.0	$Ca(m)(H_2O)_2 \cdot H_2O$ (**5**)[b] I^0O^2 2/1 226.9
60	$Ca(L)(H_2O)_2 \cdot 2H_2O$ (**1**) I^0O^3 2/2 234.6	$Ca(DL)(H_2O)_4$ (**3**) I^0O^1 4/0 243.0	$Ca(m)(H_2O)_2 \cdot H_2O$ (**5**) I^0O^2 2/1 226.9
100	$Ca(L)(H_2O)_2 \cdot 2H_2O$ (**1**) Ca(L) (**2**)	$Ca(DL)(H_2O)_4$ (**3**) I^0O^1 4/0 243.0	$Ca(m)(H_2O)_2$ (**6**) − 2 −
125	Ca(L) (**2**) I^1O^2 0/0 137.8	$Ca(DL)(H_2O)_4$ (**3**) I^0O^1 4/0 243.0	Ca(*m*) (**7**) I^1O^2 0/0 140.9
150	Ca(L) (**2**) I^1O^2 0/0 137.8	$Ca(DL)(H_2O)_4$ (**3**) $[Ca(DL)]_2 \cdot H_2O$ (**4**)	Ca(*m*) (**7**) I^1O^2 0/0 140.9
180	Ca(L) (**2**) I^1O^2 0/0 137.8	$Ca(DL)(H_2O)_4$ (**3**) $[Ca(DL)]_2 \cdot H_2O$ (**4**)	Ca(*m*) (**7**) I^1O^2 0/0 140.9
200	Ca(L) (**2**) I^1O^2 0/0 137.8	$[Ca(DL)]_2 \cdot H_2O$ (**4**) − 0.5 −	Ca(*m*) (**7**) I^1O^2 0/0 140.9
220	Ca(L) (**2**) I^1O^2 0/0 137.8	$[Ca(DL)]_2 \cdot H_2O$ (**4**) − 0.5 −	Ca(*m*) (**7**) I^1O^2 0/0 140.9

[a] All products are phase pure except where two phases are listed. The table lists composition (Tar = $C_4H_4O_6^{2-}$), connectivity, bound/free waters, and vol ($Å^3$)/mol of metal. We were not able to obtain single-crystal structures of phases **4** and **6** and thus do not know if the waters are bound or free. [b] Phases **1**[27,28] and **5**[29] have been previously described in the literature. [c] Compound **3** has been previously cited in the literature[30,31] and is commercially available (TCI), but no characterization has been reported.

three forms of tartaric acid (Table 2). Although we were unable to obtain a single crystal of the high-temperature phase, $[Ca(D,L\text{-}Tar)]_2 \cdot H_2O$ (**4**), we were able to confirm by powder X-ray diffraction (PXRD) that it does not match any of the other calcium phases or mixtures thereof. The reaction with L-tartaric acid yields pure Ca(L-Tar) (**2**), even at 220 °C. Circular dichroism spectroscopy confirms that there is no formation of a racemic conglomerate, that is, a mechanical mixture of enantiopure phases, e.g., Ca(L-Tar)/Ca(D-Tar). Neither is there significant racemization of the tartrate ligand (see Supporting Information).

Calcium Tartrate Structures. Only the structures of the two anhydrous phases, Ca(L-Tar) (**2**) and Ca(*m*-Tar) (**7**), that are used in the computational and calorimetric studies are described. The structure of $Ca(D,L\text{-}Tar)(H_2O)_4$ (**3**), experimental procedures, and characterization of all new phases are fully described in the Supporting Information.

Structure of [Ca(L-Tar)] (2). Anhydrous Ca(L-Tar) (**2**) crystallizes in the chiral space group $C222_1$ as a 3-D framework, with I^1O^2 connectivity. The asymmetric unit consists of the metal center, which lies on a special position on the two-fold rotation axis, and half a tartrate ion. The tartrate ligand overall is μ_5,κ^6, bridging five metal ions and bound through each of its six oxygen atoms (Figure 2a). The metal center is eight-coordinate bound by three bis-chelating and two monodentate tartrates. The extended structure is 3-D, connected along the *c*-axis by 1-D zigzag chains of edge-sharing M−O−M polyhedra (Figure 2b,d). Tartrate linkages to six adjacent chains along the *a* and *b* directions complete the 3-D network (Figure 2c). The average M−O bond distance is 2.465 Å. The longest M−O bond, 2.597 Å, is to the bridging carboxylate oxygen, which must accommodate two adjacent metal ions. The shortest M−O bond, 2.384 Å, is to the relatively unhindered hydroxy oxygen. M−O bond lengths are similar to those for other Ca tartrates, as are the bond lengths and angles within the tartrate ligand itself. No potential hydrogen bonds were identified.

Structure of [Ca(*meso*-Tar)] (7). The achiral *meso*-tartaric acid (*R*,*S*-tartaric acid) forms a 3-D framework with Ca, crystallizing in the space group *C*2/*c*. Like Ca(L-Tar), the *meso* phase is an anhydrous framework with I^1O^2 connectivity. The asymmetric unit contains one metal and one tartrate ligand. Each tartrate ligand is μ_5,κ^6, bound to five metal centers through all six of the oxygens (Figure 3a), and each metal is eight-coordinate. The M−O−M polyhedra form 1-D edge-sharing chains that extend along the [101] axis (Figure 3b). Each chain is connected by tartrate linkages to the six surrounding chains (Figure 3c). The average Ca−O bond lengths are typical, 2.476 Å. The shortest and longest Ca−O bonds are 2.384 and 2.684 Å to carboxylate oxygens, very similar to the bond lengths found in Ca(L-Tar) (**2**). Two crystallographically unique hydrogen bonds exist, between the hydroxy groups and carboxylate oxygens (Figure 3d). The bond lengths and angles within the tartrate ligand are unexceptional. The only major difference in tartrate geometry between the *meso* and L-tartrate phases is the C−C−C−C dihedral angle, which is 63.4° in Ca(*m*-Tar) and 33.8° in Ca(L-Tar). However, dihedral angles vary widely in known alkaline earth tartrate structures, independent of the tartrate diastereomer. The dihedral angles in Ca(L-Tar) and Ca(*m*-Tar) are both well within this range.

Structural Trends. In terms of hydration and connectivity, the overall phase behavior is fairly typical of hybrid frameworks (see Table 2). Increasing reaction temperatures yield less hydrated phases and generally higher connectivity, as expected.[13] In the L-tartrate series, the hydration decreases from four waters per metal atom in the low-temperature phase (**1**) to an anhydrous phase (**2**) at high temperatures. Although the overall connectivity is 3-D in both phases, the inorganic connectivity increases from 0-D to 1-D with the increase in temperature. The low-temperature D,L-tartrate phase, **3**, is a tetrahydrate, while the high-temperature phase, **4**, is a hemihydrate. In the *meso* system the trend in hydration is maintained. The lowest temperature phase, **5**, contains three waters; the intermediate phase, **6**, contains two waters; and the high-temperature phase, **7**, is anhydrous. In the *meso* system, both overall and inorganic connectivity increase from the low- to high-temperature phase. Overall connectivity increases from 2-D in **5** to 3-D in **7**, and inorganic connectivity increases from 0-D to 1-D.

1.2. Strontium Tartrates. The reactions between strontium acetate and tartaric acid yield six new phases from room temperature to 200 °C (Table 3).

In the strontium system, we were surprised to observe "disappearing polymorphs" [33] of two of the low-temperature phases. The observed "disappearing" phases are actually pseudopolymorphs; that is, the essential composition, Sr(L-Tar), is the same, but the phases differ in level of hydration. Initial experiments at room temperature and 60 °C yielded $Sr(L\text{-}Tar)(H_2O)_2 \cdot 2H_2O$ (**8**) and $Sr(L\text{-}Tar)(H_2O)$ (**10**), respectively. The initial room-temperature phase, **8**, which is isostructural to the known room-temperature calcium phase, **1**, has been reported in the literature and the structure determined.[22,32] The mono-

(32) Bohandy, J.; Murphy, J. C. *Acta Crystallogr., Sect.B: Struct. Cryst. Cryst. Chem.* **1968**, *24*, 286.
(33) Dunitz, J. D.; Bernstein, J. *Acc. Chem. Res.* **1995**, *28*, 193.

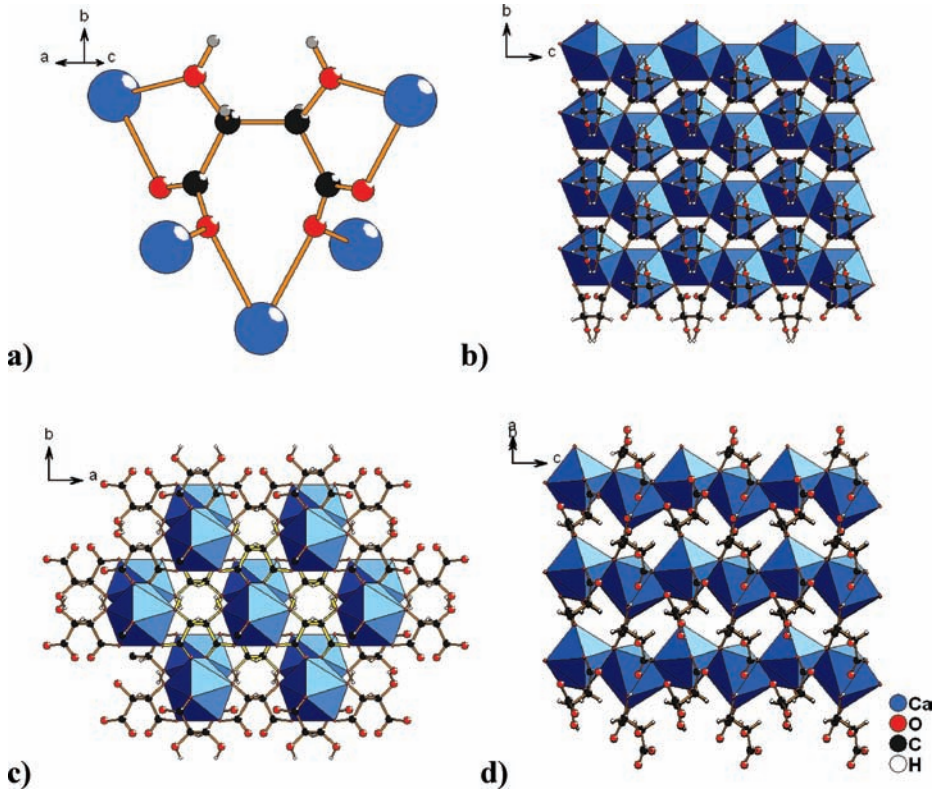

Figure 2. Views of Ca(L-Tar) (**2**). (a) Metal−tartrate coordination. (b) View down the *b*-axis, showing the 1-D edge-sharing chains of M−O−M polyhedra. (c) View down the *c*-axis, showing (yellow bonds) the tartrate ligands linking each M−O−M chain to six others. (d) Alternate view of the M−O−M chains, looking at the (−19 32 0) plane.

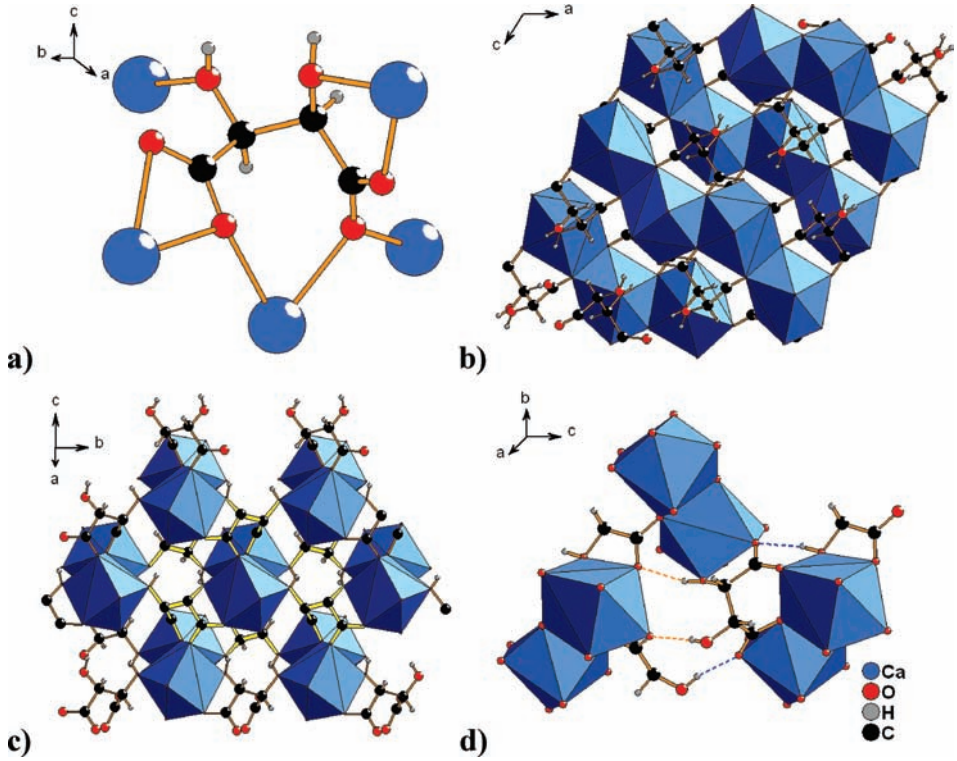

Figure 3. Views of Ca(*m*-Tar) (**7**). (a) Metal−tartrate coordination. (b) View down the *b* axis, showing the 1-D edge-sharing M−O−M chains. (c) View down the [101] axis, showing the tartrate ligands (yellow bonds) linking each M−O−M chain to six others. (d) Hydrogen bonding showing two crystallographically unique hydrogen bonds (yellow dashed bonds). Dashed bonds in blue are symmetry equivalent to yellow bonds.

hydrate Sr(L-Tar)(H_2O) (**10**) is a new phase and was fully characterized, including a single-crystal structure. Both phases were synthesized numerous times over a period of months. However, at the end of this period, a reaction at 60 °C, under

Table 3. Reactions between $Sr(OAc)_2$ and Tartaric Acid[a]

temp (°C)	Sr		
	L-Tar (L)	D,L-Tar (DL)	*meso*-Tar (*m*)
rt	$Sr(L)(H_2O)_2 \cdot 2H_2O$ (**8**)[b,c] I^0O^3 2/2 249.3	$Sr(DL)(H_2O)_4$ (**12**) I^0O^1 4/0 255.1	Sr(*m*) (**13**) I^1O^2 0/0 152.1
60	$Sr(L)(H_2O)$ (**10**)[c] I^1O^2 1/0 182.7	$Sr(DL)(H_2O)_4$ (**12**) I^0O^1 4/0 255.1	Sr(*m*) (**13**) I^1O^2 0/0 152.2
100	$Sr(L)(H_2O)$ (**10**) Sr(L) (**11**)	$Sr(DL)(H_2O)_4$ (**12**) I^0O^1 4/0 255.1	Sr(*m*) (**13**) I^1O^2 0/0 152.3
125	Sr(L) (**11**) I^1O^2 0/0 148.9	$Sr(DL)(H_2O)_4$ (**12**) I^0O^1 4/0 255.1	Sr(*m*) (**13**) I^1O^2 0/0 152.4
150	Sr(L) (**11**) I^1O^2 0/0 148.9	$Sr(DL)(H_2O)_4$ (**12**) Sr(*m*) (**13**)	Sr(*m*) (**13**) I^1O^2 0/0 152.5
180	Sr(L) (**11**) Sr(*m*) (**13**)	$Sr(DL)(H_2O)_4$ (**12**) Sr(*m*) (**13**)	Sr(*m*) (**13**) I^1O^2 0/0 152.6
200	Sr(*m*) (**13**) I^1O^2 0/0 152.5	Sr(m) (**13**) I^1O^2 0/0 152.6	Sr(m) (**13**) I^1O^2 0/0 152.7

[a] All products are phase pure except where two phases are listed. The table lists composition (Tar = $C_4H_4O_6^{2-}$), connectivity, bound/free waters, and vol (Å^3)/mol of metal. [b] Phase **8** has been previously reported in the literature.[22,32] [c] Disappearing pseudopolymorphs. Later experiments yielded the known phase[20] Sr(L-Tar)$(H_2O)_3$ (**9**).

identical experimental conditions to the original syntheses but using a lower purity sample of D-tartaric acid, rather than L-tartaric acid, was performed. Instead of yielding the expected product, Sr(D-Tar)(H_2O) (**10**), the reaction yielded the pseudopolymorph, Sr(D-Tar)$(H_2O)_3$ (**9**). Subsequent to this synthesis of **9**, the original phases, **8** and **10**, could no longer be obtained under the original conditions. The pseudopolymorph Sr(D-Tar)$(H_2O)_3$ (**9**) has been previously reported in the literature as the sole product at room temperature, and the structure has been solved.[20,34] We suspect that impurities present in the D-tartaric acid reagent were key in initiating the formation of the "dominant" pseudopolymorph, **9**, which subsequently represses formation of the metastable pseudopolymorphs, **8** and **10**.[33] For more details, see the Supporting Information.

Four of the calcium and strontium phases are isostructural: the room-temperature phases M(L-Tar)$(H_2O)_2 \cdot 2H_2O$ (**1**, Ca and **8**, Sr), the D,L phases M(D,L-Tar)$(H_2O)_4$ (**3**, **12**), and both the L and *meso* anhydrous phases, M(L-Tar) (**2**, **11**) and M(*m*-Tar) (**7**, **13**).

Phase Behavior. Although the anhydrous phases of calcium and strontium are isostructural, the high-temperature phase behavior of the strontium tartrates is strikingly different than that of calcium. At a synthesis temperature of 200 °C, reaction with any of the three forms of tartaric acid yields a single product, the anhydrous *meso* phase, Sr(*m*-Tar) (**13**). Furthermore, both the L phase, Sr(L-Tar) (**11**), and the D,L phase, Sr(D,L-Tar)$(H_2O)_4$ (**12**), can be converted to Sr(*m*-Tar) by hydrothermal treatment of a suspension at 200 °C over several days. The reaction of strontium and tartaric acid at high temperatures is clearly under thermodynamic control, and the *meso* phase, **13**, is the most thermodynamically stable phase.

From the experimental work it is not possible to determine if the *meso* phase is the most thermodynamically stable at all temperatures, because in order to form the *meso* phase from L- or D,L-tartaric acid, the isomerization of tartaric acid is required. Tartaric acid does not racemize rapidly at low temperatures, so at lower temperatures it may be the kinetic barrier to isomerization, rather than thermodynamic control, that determines phase formation. Alternatively, the *meso* phase may only be the thermodynamically stable phase at higher temperatures, due to entropic contributions that only become significant as the temperature increases. These two scenarios cannot be easily differentiated by synthetic experiments. For this reason, and to better understand the different high-temperature phase behaviors of the isostructural calcium and strontium systems, we undertook both computational and calorimetric studies on the anhydrous calcium and strontium phases, which will be described later.

Strontium Tartrate Structures. Only the anhydrous phases, Sr(L-Tar) (**11**) and Sr(*m*-Tar) (**13**), that are used in the computational and calorimetry studies are described. Full structural descriptions of the new phases **10** and **12**, as well as experimental procedures and characterization of all new phases, are included in the Supporting Information.

Structure of Sr(L-Tar) (11). The anhydrous phase Sr(L-Tar) is isostructural to Ca(L-Tar) (**2**). The only major differences are in the M−O bond lengths, which are uniformly longer in the strontium phase, as expected. The average M−O bond distance is 2.566 Å in Sr(L-Tar). The longest and shortest M−O bonds are 2.637 and 2.514 Å, respectively. M−O bond lengths are similar to those in other strontium tartrates. The bond lengths and angles within the tartrate ligand itself are normal. No potential hydrogen bonds were identified.

Structure of Sr(*meso*-Tar) (13). The anhydrous phase Sr(*m*-Tar) is also isostructural to the calcium phase, Ca(*m*-Tar). Again only the M−O bond lengths are different. The average M−O bond length is 2.587 Å, and the longest and shortest bonds are 2.747 and 2.516 Å, respectively. Two crystallographically unique hydrogen bonds exist, between the hydroxy groups and carboxylate oxygens. The bond lengths and angles of the tartrate ligand are standard. As in the calcium tartrates, the geometry of the tartrate ligand in Sr(L-Tar) versus Sr(*m*-Tar) only differs significantly in the C−C−C−C dihedral angles, which are 35.2° and 62.4°, respectively. The dihedral angles in each are substantially similar to those in the respective isostructural calcium phases.

Structural Trends. The strontium tartrates also follow the expected trends in terms of hydration and connectivity (see Table 3). The hydration in the L-tartrate phases decreases from 4 to 3 to 1 to 0 water molecules per Sr with increasing temperature. The overall connectivity for all the L-tartrate phases is 3-D, but inorganic connectivity increases from 0-D to 1-D with an increase in synthesis temperature.

Only Sr(L-Tar)(H_2O) (**10**) maintained crystallinity with loss of water, forming the high-temperature phase Sr(L-Tar) (**11**) on dehydration, as shown by variable-temperature PXRD (see Supporting Information). The transformation of **10** to **11** requires loss of a coordinated water and a major rearrangement of the metal−tartrate coordination (Figure 4). All other strontium hydrate phases became amorphous on dehydration.

Solid Solutions: Strontium and Calcium. The strontium and calcium L-Tar phases, Sr(L-Tar) (**11**) and Ca(L-Tar) (**2**), form infinite solid solutions at 150 °C with the lattice parameters

(34) Arora, S. K.; Patel, V.; Kothari, A.; Amin, B. *Cryst. Growth Des.* **2004**, *4*, 343.

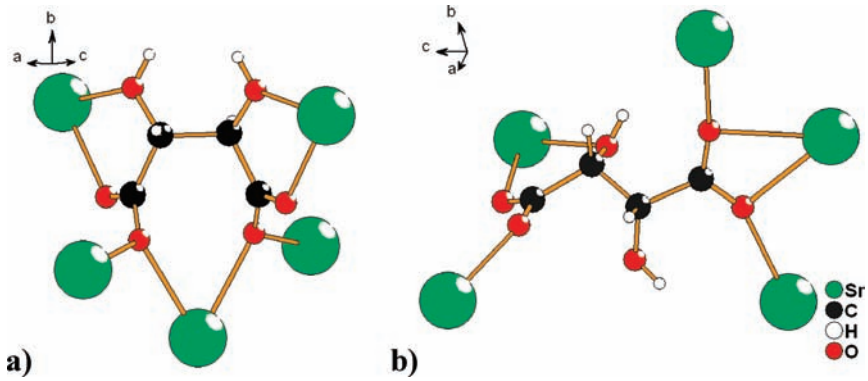

Figure 4. Coordination of tartrate ligand in (a) Sr(L-Tar) (**11**) and (b) Sr(L-Tar)(H_2O) (**10**), showing the rearrangement that occurs on dehydration of **10** to yield **11**.

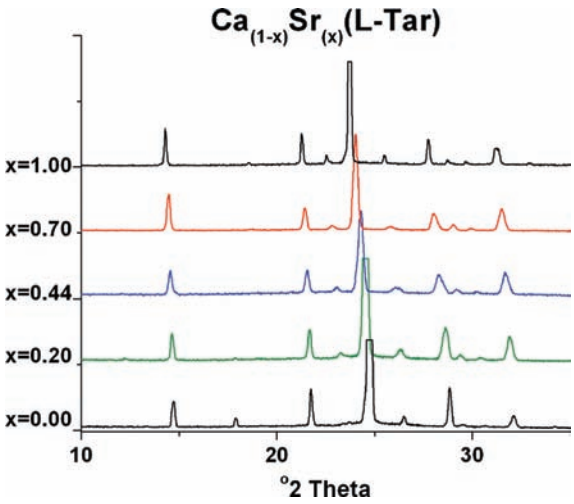

Figure 5. Powder X-ray diffraction patterns of $Ca_{(1-x)}Sr_{(x)}$(L-Tar) solid solutions. The largest peak, at ~25° 2θ, has been truncated in the bottom three plots for clarity. The full diffraction patterns (0−60° 2θ) are included in the Supporting Information.

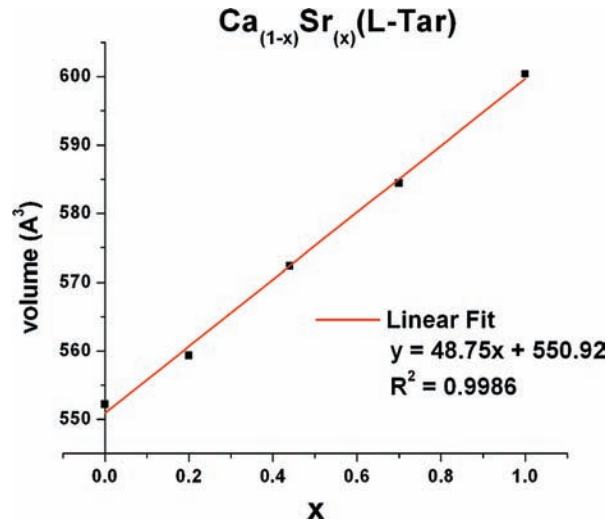

Figure 6. Plot of volume (Å^3) versus composition for $Ca_{(1-x)}Sr_{(x)}$(L-Tar) solid solutions. Cell parameters were determined by Reitveld refinement using GSAS/EXPGUI,[35,36] and composition was determined by ICP.

following Vegard's law (Figures 5 and 6). Solid solution formation at other temperatures was not studied.

1.3. Barium Tartrates. The reactions between barium acetate and tartaric acid from room temperature to 220 °C (Table 4) form five unique phases. The barium tartrates are less diverse than the calcium and strontium systems. In fact, only D,L-tartaric acid forms more than one phase with barium over the temperature range studied.

Phase Behavior. All three D,L phases form at room temperature, and the composition of the final mixture is highly sensitive to small variations in reaction conditions. Most often the room-temperature reaction yields mixtures of all three phases, but occasionally mixtures of only two phases are observed. Above 60 °C the only phase formed is the anhydrous phase, Ba(D,L-Tar) (**17**).

The high-temperature phase behavior of the barium tartrates is more complex than that of calcium or strontium. At 200 °C and above the reaction with *meso*-tartaric acid yields Ba(D,L-Tar) (**17**), and a suspension of the *meso* phase Ba(*m*-Tar)(H_2O) (**18**) can be converted to Ba(D,L-Tar) by hydrothermal treatment at 220 °C over several days. Thus, Ba(D,L-Tar) is clearly the thermodynamic product relative to Ba(*m*-Tar)(H_2O) above 200 °C.

The reaction with L-tartaric acid also yields mixtures of Ba(L-Tar) (**14**) and Ba(D,L-Tar) at 220 °C. Pure Ba(D,L-Tar) can be obtained starting from L-tartaric acid at 220 °C at low concentrations (0.5 mM) and over long reaction times (5 days). These observations suggest that, at 200 °C and above, Ba(D,L-Tar) is the thermodynamically most stable phase. The formation of the Ba(D,L-Tar) phase as the product of the reaction with D,L-tartaric acid, rather than formation of a racemic conglomerate of the Ba(L-Tar)/Ba(D-Tar) phase, supports this conclusion.

However, at our normally used concentrations (1 mM), pure Ba(D,L-Tar) is never obtained from the reaction of barium and L-tartaric acid, even with long reaction times. Furthermore, treatment of a suspension of Ba(L-Tar) at 220 °C for days leaves the sample unchanged. These results suggest that, at these concentrations, the Ba(L-Tar) phase is the kinetic product of the reaction and must have a sufficiently high barrier to conversion to Ba(D,L-Tar) that the latter can not form under the conditions studied. One possible scenario is that rapid formation and precipitation of a highly insoluble kinetic product, e.g., Ba(L-Tar), precludes formation of the thermodynamic

(35) Larson, A. C.; Von Dreele, R. B. *General Struture Analysis System (GSAS) Manual*; Los Alamos National Laboratory Report LAUR 86-748; Los Alamos National Laboratory: Los Alamos, NM, 2000.
(36) Toby, B. H. *J. Appl. Crystallogr.* **2001**, 34.

Table 4. Reactions between $Ba(OAc)_2$ and Tartaric Acid[a]

temp (°C)	Ba		
	L-Tar (L)	D,L-Tar (DL)	*meso*-Tar (*m*)
rt	Ba(L) (**14**)[b] I^1O^2 0/0 155.1	$Ba_2(DL)_2(H_2O)_5$ (**15**) I^1O^1 2.5/0 216.0 $Ba(DL)(H_2O)_2$ (**16**) I^1O^1 2/0 213.9 Ba(DL) (**17**)	Ba(*m*)(H_2O) (**18**) I^1O^2 1/0 185.1
60	Ba(L) (**14**) I^1O^2 0/0 155.1	Ba(DL) (**17**) I^3O^0 0/0 152.6	Ba(*m*)(H_2O) (**18**) I^1O^2 1/0 185.1
100	Ba(L) (**14**) I^1O^2 0/0 155.1	Ba(DL) (**17**) I^3O^0 0/0 152.6	Ba(*m*)(H_2O) (**18**) I^1O^2 1/0 185.1
125	Ba(L) (**14**) I^1O^2 0/0 155.1	Ba(DL) (**17**) I^3O^0 0/0 152.6	Ba(*m*)(H_2O) (**18**) I^1O^2 1/0 185.1
150	Ba(L) (**14**) I^1O^2 0/0 155.1	Ba(DL) (**17**) I^3O^0 0/0 152.6	Ba(*m*)(H_2O) (**18**) I^1O^2 1/0 185.1
180	Ba(L) (**14**) I^1O^2 0/0 155.1	Ba(DL) (**17**) I^3O^0 0/0 152.6	Ba(*m*)(H_2O) (**18**) I^1O^2 1/0 185.1
200	Ba(L) (**14**) I^1O^2 0/0 155.1	Ba(DL) (**17**) I^3O^0 0/0 152.6	Ba(*m*)(H_2O) (**18**) Ba(DL) (**17**)
220	Ba(L) (**14**) Ba(DL) (**17**)	Ba(DL) (**17**) I^3O^0 0/0 152.6	Ba(*m*)(H_2O) (**18**) Ba(DL) (**17**)

[a] All products are phase pure except where two phases are listed. The table lists composition (Tar = $C_4H_4O_6^{2-}$), connectivity, bound/free waters, and vol ($Å^3$)/mol of metal. [b] Phase **14** has been previously described in the literature.[21]

product, e.g., Ba(D,L-Tar), except at very low concentrations where precipitation of the kinetic product is no longer favorable. This scenario would explain our experimental observations at high and low concentrations.

The high-temperature barium reactions appear to be controlled by both thermodynamic and kinetic factors. The reactions with L-tartaric acid at higher concentrations are under kinetic control, and Ba(L-Tar) is formed. When concentration disfavors initial formation of Ba(L-Tar), the thermodynamically stable product, Ba(D,L-Tar), is observed. At low temperatures we cannot determine, from the synthetic results, if the phase behavior is controlled by the same factors. The relative phase stabilities at low temperature may be different than at high temperature, or the isomerization/racemization of tartaric acid may play a key kinetic role. These questions will be addressed in the discussion of the computational and calorimetric studies.

Barium Tartrate Structures. Only the anhydrous phases, Ba(L-Tar) (**14**) and Ba(D,L-Tar) (**17**), used in the computational and calorimetric studies are described. Full structural descriptions of **15**, **16**, and **18**, and experimental procedures and characterization of all new phases are included in the Supporting Information.

Structure of [Ba(L-Tar)] (14). The structure of **14** was solved by Torres,[21] but we will briefly describe it here in the terms we have used for the previous compounds. Compound **14** crystallizes in the chiral space group $P2_12_12_1$. The tartrate ligand is μ_6,κ^6 (Figure 7a). The barium is nine-coordinate, and the overall connectivity is 3-D. The M−O−M connectivity is only 1-D, with the Ba−O polyhedra forming chains of face-sharing polyhedra along the *c*-axis (Figure 7b,c). The average Ba−O distance is 2.816 Å, and the shortest and longest bonds are 2.769 and 2.875 Å. Although two crystallographically unique hydrogen bonds are reported in the previous work, one of the reported H-bonds has a very small D−H−A angle (128°) and, therefore, in this work is not included. We consider the structure to contain a single crystallographically unique hydrogen bond, between a hydroxy and carboxylate oxygen (Figure 7d).

Structure of [Ba(D,L-Tar)] (17). Compound **17** crystallizes in $P2_1/c$, and the asymmetric unit is made up of one barium atom and one tartrate ligand. The tartrate ligand is μ_6,κ^6, bound through each oxygen to six barium atoms (Figure 8a). The barium atom is 10-coordinate, and the structure is a rare example of 3-D M−O−M connectivity (I^3O^0). Each barium atom is connected by two bridging oxygen atoms to four adjacent barium atoms in a pseudotetrahedral arrangement (Figure 9a). The resulting 3-D structure of edge-sharing M−O−M polyhedra is further interconnected by tartrate ligands, leading to a very complex overall structure (Figure 8b). The average Ba−O bond distance is 2.889 Å, and the shortest and longest bonds are 2.647 and 3.078 Å. Interestingly, the overall arrangement of the barium atoms is diamondoid (Figure 9). The L- and D-enantiomers of the tartrate ligand segregate within the crystal, forming alternating corrugated layers in the *ab* plane (Figure 8c). One crystallographically unique hydrogen bond exists, between a hydroxy group and carboxylate oxygen (Figure 8d).

Structural Trends. The *meso* and L-tartrate barium compounds form only a single phase, but the multiple phases of the barium D,L-tartartes follow the expected trends in connectivity and hydration (see Table 4). The hydration decreases from 2−2.5 in the low-temperature phases to 0 in the high-temperature phase, and both inorganic and overall connectivity increase with increasing temperature. The overall connectivity increases from 2-D to 3-D, and the inorganic connectivity increases from 1-D to 3-D.

Solid Solutions: Barium and Strontium. Although the pure phases are not isostructural, barium and strontium form partial solid solutions in reaction with *meso*-tartaric acid at 60 °C (Figure 10). The structure of the Ba(*m*-Tar)(H_2O) (**18**) phase is described in detail in the Supporting Information. Over the range of $x = 0$ to $x \approx 0.1$, a solid solution of the anhydrous strontium phase, $Sr_{(1-x)}Ba_{(x)}$(*m*-Tar), exists. Between $x \approx 0.1$ and $x \approx 0.2$ there is a two-phase region, and from $x = 0.2$ to $x = 1.0$ there is a second solid solution region of the barium phase, $Sr_{(1-x)}Ba_{(x)}$(*m*-Tar)(H_2O). It is interesting that the strontium forms an extensive solid solution with the barium hydrate, Ba(*m*-Tar)(H_2O), even though the analogous phase Sr(*m*-Tar)(H_2O) does not form under the conditions studied. Likewise, barium forms a solid solution with the anhydrous strontium *meso* phase, although over a much smaller range of compositions, even though no anhydrous barium *meso* phase forms below 220 °C. The hydrate Ba(*m*-Tar)(H_2O) does convert to a new high-temperature phase on dehydration (see Supporting Information), but this phase is not isostructural to the anhydrous strontium phase.

2. Computational and Calorimetric Studies. In order to better understand the differences in high-temperature phase behavior between the Ca, Sr, and Ba systems, we determined the relative stabilities of the anhydrous high-temperature phases by computational methods[37−39] and acid solution calorimetry (Table 5) (see Supporting Information for additional details). The hydrated phases, Ca- and Sr(D,L-Tar)$(H_2O)_4$ (**3** and **12**) and Ba(*m*-Tar)(H_2O) (**18**), were not considered in this part of the

(37) *CP2K*, http://cp2k.berlios.de.
(38) VandeVondele, J.; Krack, M.; Mohamed, F.; Parrinello, M.; Chassaing, T.; Hutter, J. *Comput. Phys. Commun.* **2005**, *167*, 103.
(39) Krack, M.; Parrinello, M. *Forschungs. Jülich, NIC Ser.* **2004**, *25*, 29.

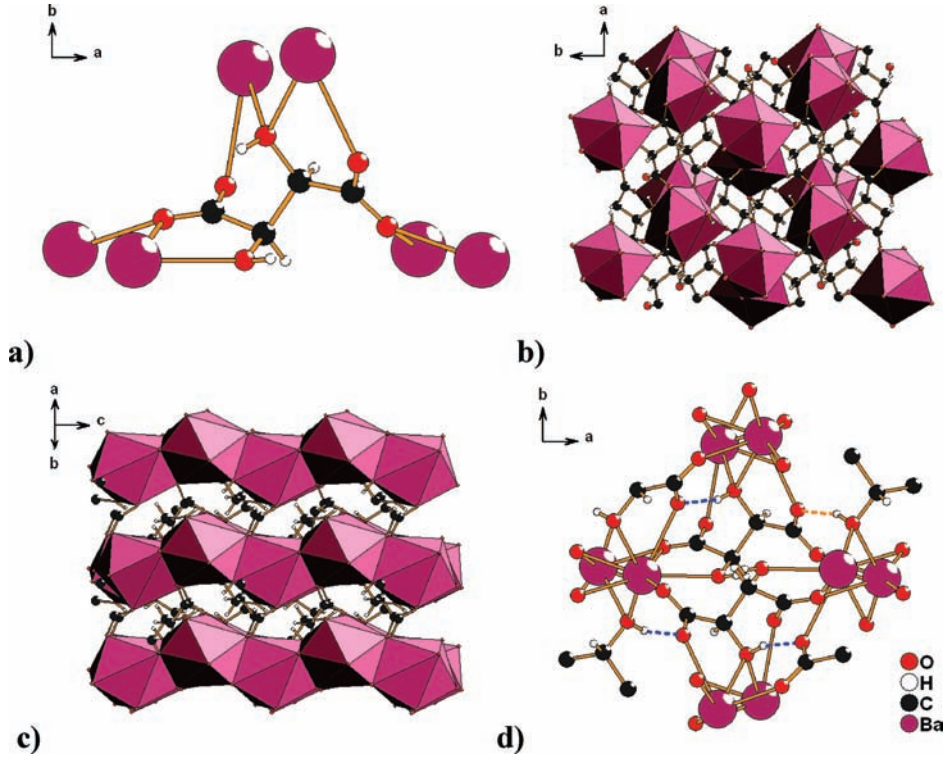

Figure 7. Views of Ba(L-Tar) (**14**). (a) Metal−tartrate coordination. (b) View down the *c* axis showing an end view of the 1-D M−O−M chains. (c) View down the [101] axis showing the M−O−M chains. (d) Hydrogen bonding showing one crystallographically unique bond (dashed yellow bonds). Dashed bonds in blue are symmetry equivalents.

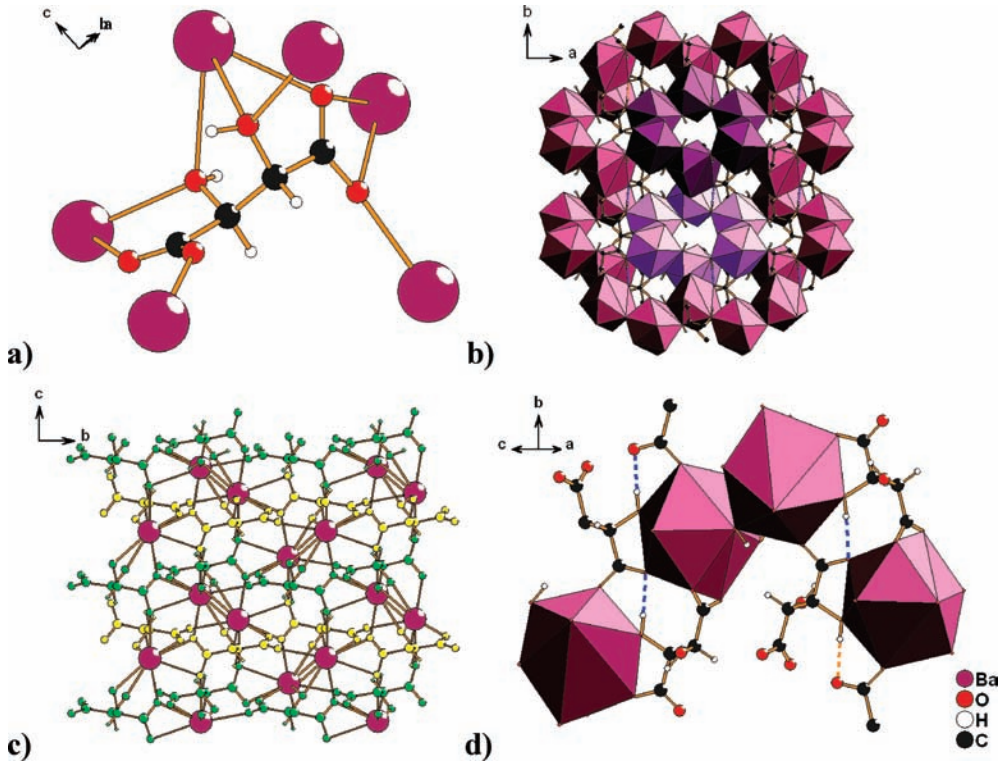

Figure 8. Views of Ba(D,L-Tar) (**17**). (a) Metal−tartrate coordination. (b) View of M−O polyhedra with two of the six-membered M−O−M rings tinted as a visual aid. (c) View of the structure down the *a* axis showing segregation of the L- (yellow) and D-tartrates (green) into separate layers. (d) Hydrogen bonding showing one crystallographically unique hydrogen bond (dashed yellow bond) from a hydroxy group to a carboxylate oxygen. Dashed blue bonds are symmetry-equivalent hydrogen bonds.

study because of the difficulty in comparing the energetics of phases with different stoichiometries by computational methods.

In the calcium system the computational work predicted that the Ca(*m*-Tar) phase, **7**, would be more stable in total electronic

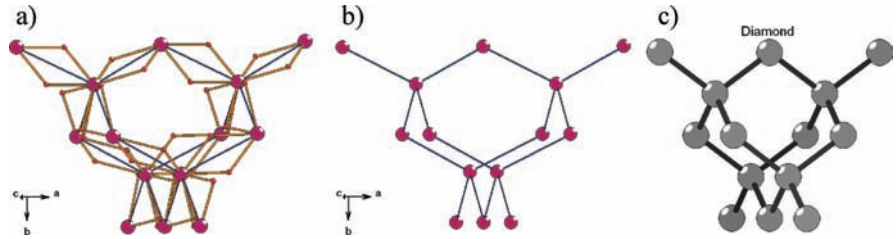

Figure 9. Diamondoid arrangement of the barium atoms in Ba(D,L-Tar) (a) with and (b) without bridging oxygens, and (c) the diamond unit cell. Nonbridging oxygens in (a) are excluded for clarity. Each metal center in the diamondoid structure is bridged by two oxygens to each of four adjacent bariums, in a pseudotetrahedral geometry.

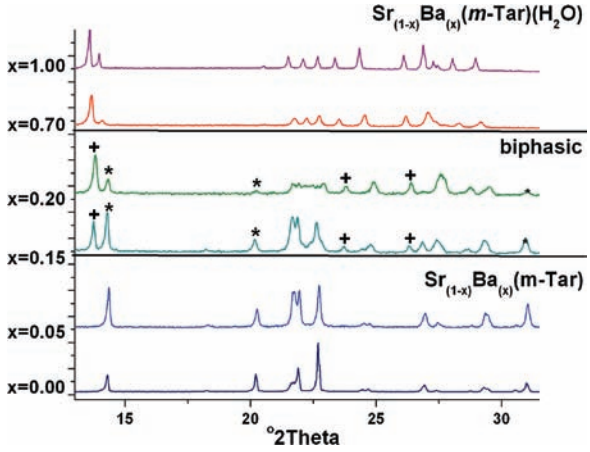

Figure 10. Powder X-ray diffraction patterns of solid solutions of $Sr_{(1-x)}Ba_{(x)}$(*m*-Tar)(H_2O) and $Sr_{(1-x)}Ba_{(x)}$(*m*-Tar). In the biphasic region, the + symbol indicates characteristic peaks of the Ba(*m*-Tar)(H_2O) phase; the * symbol indicates characteristic peaks of the Sr(*m*-Tar) phase.

Table 5. Total Electronic Energies, Enthalpies of Solution, and Relative Stabilities of Phases As Determined by Computational Methods (CP2K) and Acid Solution Calorimetry

phase	total electronic energy, calculated (kJ/mol)	enthalpy of solution, calorimetry (kJ/mol)	relative stabilities	
			calculated (kJ/mol)	calorimetry (kJ/mol)
Ca(*m*-Tar) (**7**)	−415478.0	−2.40 ± 0.11	0	0
Ca(L-Tar) (**2**)	−415487.1	−5.34 ± 1.63	9.1	2.9 ± 1.6
Sr(*m*-Tar) (**13**)	−399738.2	−1.79 ± 0.16	0	0
Sr(L-Tar) (**11**)	−399751.5	−9.89 ± 1.40	13.4	8.1 ± 1.4
Ba(L-Tar) (**14**)	−385962.1	8.89 ± 0.78	0	0
Ba(D,L-Tar) (**17**)	−385968.6	1.84 ± 0.57	6.4	7.0 ± 1.0

energy than the Ca(L-Tar) phase, **2**, by 9.1 kJ/mol. The calorimetric study determined the Ca(*m*-Tar) phase to be 2.9 ± 1.6 kJ/mol more stable in enthalpy than the Ca(L-Tar) phase. The Sr(*m*-Tar) phase, **13**, was also determined to be more stable than the Sr(L-Tar) phase, **11**, by both methods. Computation predicted Sr(*m*-Tar) to be more stable by 13.4 kJ/mol, while by acid calorimetry the difference was determined to be 8.1 ± 1.4 kJ/mol. In the barium system the computational and calorimetric results also agreed. Both methods determined the chiral Ba(L-Tar) phase, **14**, to be more stable, by 6.4 and 7.0 ± 1.0 kJ/mol for computational and calorimetric methods, respectively.

A notable result of this study is the excellent agreement between computational and calorimetric results. Although the numerical values of the relative stabilities determined by computational and calorimetric studies are not identical, they are quite similar, and in all three cases the computational work correctly identified the most stable phase. This is especially notable in light of the very small differences in stabilities relative to the total energies. These results are an excellent demonstration of the effectiveness of advanced DFT methods[37−40] as applied to complex extended structures, such as metal−organic frameworks, as well as the accuracy of modern acid solution calorimetry.

Note that the computational work refers to total electronic energy,[41] while the calorimetric studies determine enthalpies. Because the volume changes of the transformations are small and the pressure is low, the difference between total electronic energy and enthalpy can be neglected. Furthermore, the calorimetric data refer to room temperature, while the computations determine total electronic energy at 0 K. Differences in heat capacities, related to differences in lattice vibrations, will make these values differ slightly, but the effect is not expected to be significant. Thermodynamic stability is, of course, determined by the free energy, which requires knowledge of the entropy. Therefore, the experimentally observed phase stabilities may not match the computationally and calorimetrically determined phase sequence of energies, especially at high temperatures where the entropic contribution to the free energy may be significant.

The energetics provide insight into the different phase behavior of the isostructural Ca and Sr systems. Experimentally we observe that Sr(L-Tar) (**11**) converts to Sr(*m*-Tar) (**13**) at 200 °C, but Ca(L-Tar) (**2**) never converts to Ca(*m*-Tar) (**7**), even up to 220 °C. The isostructural *meso* phases Ca(*m*-Tar) and Sr(*m*-Tar) are both found to be lower in enthalpy/total electronic energy than the respective isostructural L phases, Ca(L-Tar) and Sr(L-Tar), by computational and calorimetric methods. Significantly, both methods also determine that the difference in enthalpy/total electronic energy of the *meso* phase compared to the L phase is larger for the strontium phases than the calcium phases. The greater difference in relative stability, providing a greater thermodynamic driving force for transformation, may explain why the *meso* phase is observed as the single thermodynamic product in the strontium system, but not in the calcium system. The thermodynamic data suggest that in both systems the *meso* phases, which are lower in enthalpy/total electronic energy than the L phases, should be the thermodynamic product at low temperatures. Furthermore, if the *meso* phases are higher in entropy than the L phases, then the data imply that the L phases are metastable under all conditions. However, conversion

(40) VandeVondele, J.; Hutter, J. *J. Chem. Phys.* **2007**, *127*, 114105.
(41) The zero-point vibrational energies (ZPVEs) are not included in the calculations. Addition of the ZPVE is not expected to change the relative stabilities of the calculated phases. See: Rivera, S. A.; Allis, D. G.; Hudson, B. S. *Cryst. Growth Des.* **2008**, *8*, 3905.

to the *meso* phase appears to be controlled by kinetics, perhaps involving a barrier to isomerization of the tartaric acid. The kinetic barrier precludes isomerization of the L to *meso* phases at low temperatures. In the Sr system the kinetic barrier is overcome above 180 °C and conversion of Sr(L-Tar) to Sr(*m*-Tar) is observed, whereas in the Ca system there is no conversion below 220 °C. The rate of isomerization may be affected by many factors, including aqueous solubility and the nature of the metal ion.

The interplay of kinetic and thermodynamic factors is evident in the barium tartrate system. Both the computational and calorimetric work determined that the Ba(L-Tar) phase, **14**, is more stable in internal energy/enthalpy than the Ba(D,L-Tar) phase, **17**. However, experimentally the Ba(D,L-Tar) phase, **17**, is formed and appears to be the thermodynamically stable phase at high temperatures. This implies that the Ba(L-Tar) phase is thermodynamically stable below some transition temperature and the Ba(D,L-Tar) phase above. The calorimetrically determined enthalpy difference of 7 kJ/mol implies a transition temperature of 1215 K. To obtain a transition temperature near 200 °C (473 K) as observed experimentally, one would need an entropy change of 14.8 J mol^{-1} K^{-1}.

Ba(D,L-Tar) also forms at lower temperatures, including room temperature. On the basis of the calorimetrically determined stabilities, we would expect the reaction with D,L-tartaric acid at room temperature to form a racemic conglomerate, a 50:50 mixture of Ba(L-Tar)/Ba(D-Tar). For the Ba(D,L-Tar) phase to be the thermodynamically stable phase at room temperature, the entropy of transition would have to be 23.5 J mol^{-1} K^{-1}, which is rather large. One possible explanation is that the reaction with D,L-tartaric acid at room temperature is under kinetic rather than thermodynamic control. Indeed, Brock and Dunitz[42] suggest that, from a solution of the racemate, the crystallization of a racemic phase, such as Ba(D,L-Tar), may be kinetically favored over the crystallization of the conglomerate of the enantiopure phase. The barium system aptly demonstrates the importance of energetic, entropic, and kinetic factors in controlling phase behavior.

Despite the wealth of insight that has been gained by this multifaceted approach to studying phase behavior, it is worth noting that it remains difficult to directly relate the structural details of the phases to the energetics. For example, in the Ca and Sr phases the C−C−C−C dihedral angle of the tartrate is quite different between the M(L-Tar) and M(*m*-Tar) structures, ∼35° in the M(L-Tar) structures and ∼65° in the M(*m*-Tar) structures. However, it is not clear what role, if any, the difference in C−C−C−C dihedral angles plays in determining the relative phase stabilities. Likewise, the characteristics of the metal ion clearly influence the relative stabilities, as demonstrated by the difference in relative stabilities in the isostructural Ca and Sr systems. Whether the differences are due simply to the different ionic radii or to more subtle structural differences is difficult to determine. Similarly, though there are major structural differences between the Ba(L-Tar) and Ba(D,L-Tar) phases, the energetics of the two phases are similar enough that the relative stabilities invert over a 200 °C temperature range.

In all three systems (Ca, Sr, Ba) the isomerization of tartaric acid is likely to influence the phase behavior. In the barium system no racemization or formation of the Ba(D,L-Tar) phase was observed in reaction with L-tartaric acid at temperatures below 200 °C, even at low concentrations and long reaction times. Racemization and formation of a Ba(L-Tar)/Ba(D-Tar) conglomerate was ruled out by circular dichroism (see Supporting Information). Previous work[16] has shown that a solution of sodium tartrate loses ∼50% of optical activity after 24 h of hydrothermal treatment at 200 °C and suggests that hydrothermal synthesis with tartaric acid should be limited to 3 days at 160 °C or 1 day at 180 °C. However, our results show that racemization (and isomerization to or from the *meso* diastereomer) are not consistently temperature dependent. Only in the strontium system is tartrate isomerization observed below 180 °C. There is no evidence in the barium reactions of isomerization below 200 °C, even over 5 days, and there is no evidence of any isomerization in the calcium system up to 220 °C. Likewise, in previous work on magnesium[18] no isomerization of the tartrate ligand was observed up to 200 °C. Tartrate isomerization clearly depends highly on other experimental conditions, including pH, the identity of the cation, and, possibly, the relative phase stability of the chiral and racemic or achiral phases. Thus, while the possibility of isomerization of chiral ligands certainly must be considered in the analysis of the products, high reaction temperatures and long reaction times do not necessarily result in isomerization and loss of chirality.

Conclusions

The synthesis of chiral and achiral calcium, strontium, and barium tartrates from room temperature to 220 °C was studied, yielding 18 phases over the temperature range, including 13 new phases. The high-temperature phase behavior of each metal system was different. Calcium formed a unique phase with L-, *meso*-, and D,L-tartaric acid undergoing no isomerization or phase transitions up to 220 °C. In contrast, in the reaction of Sr at temperatures above 180 °C, the Sr(*m*-Tar) phase was the sole product of the reaction with all of the tartaric acid starting materials. Likewise, in reactions with barium, the Ba(D,L-Tar) phase was the only product at synthesis temperatures above 200 °C. Determinations of the relative energetic stabilities of several phases by computational and calorimetric methods were in excellent agreement and led to a more complete understanding of the phase behavior. Furthermore, there was excellent agreement between the relative energetic stabilities obtained by computational and calorimetric means. Both the relative thermodynamic stabilities of the metal tartrate phases and kinetic factors, such as ligand racemization and phase crystallization, were determined to be key factors in controlling the phase behavior. The occurrence of ligand racemization/isomerization at high temperatures and the overall phase stability were unique for each metal tartrate system, even for the isostructural calcium and strontium tartrates. The intricate relationships between phase behavior, thermodynamic stabilities, and kinetic factors emphasize the difficulty in predicting synthetic outcomes in such systems. Nonetheless, the combination of synthetic studies, calorimetry, and computation provides a deeper understanding of these complex systems.

Acknowledgment. The authors thank J. VandeVondele (University of Zurich, Switzerland) and M. Krack (Paul Scherrer Institute, Switzerland) for useful discussions and J. VandeVondele for providing the basis sets. The computational work was performed on the supercomputer Mare Nostrum at the Barcelona Supercomputing Center−Centro Nacional de Supercomputación. The calorimetric work was supported by NSF grant DMR-0601892. L.A.

(42) Brock, C. P.; Schweizer, W. B.; Dunitz, J. D. *J. Am. Chem. Soc.* **1991**, *113*, 9811.

was supported by the Solid State Lighting and Energy Center, University of California, Santa Barbara. A.K.C. thanks the ERC for an Advanced Investigator Award. This work made use of MRL Central Facilities supported by the MRSEC Program of the NSF under award no. DMR05-20415.

Supporting Information Available: Experimental procedures and characterization of all new compounds (elemental analysis, TGA, PXRD). Crystallographic data for all new structures, including CIF files, tables of bond distances and angles, and structural descriptions of phases not detailed in the text (**3**, **10**, **12**, **15**, **16**, **18**). Detailed description of computational methods. Detailed description of calorimetry methods and additional calorimetry data on tartaric acid. Additional information on "disappearing polymorphs" as referenced in the text and on Ca/Sr and Ba/Sr solid solutions. This material is available free of charge via the Internet at http://pubs.acs.org. The supplementary crystallographic data for this paper are also deposited as CCDC 738953−738963. These data can be obtained free of charge from The Cambridge Crystallographic Data Centre via www.ccdc.cam.ac.uk/data_request/cif.

JA905690T